

## 3D Reconstruction of Underground Cable Wells with Automatic Extraction of Point Cloud Contour Lines

Ming Huang,<sup>1,2</sup> Mingyue Kuang,<sup>1\*</sup> and Rui Wu<sup>1,3</sup>

<sup>1</sup>School of Mapping and Urban Spatial Information, Beijing University of Civil Engineering and Architecture,  
Beijing 102616, China

<sup>2</sup>Engineering Research Center of Typical Architecture and Ancient Architecture Database, Beijing 102616, China

<sup>3</sup>School of Architecture Civil Engineering, Huangshan University, Huangshan 2450331, China

(Received October 25, 2024; accepted December 6, 2024)

**Keywords:** laser point cloud, underground cable wells, alpha shapes, skeleton and contour line extraction, 3D reconstruction

Accurate 3D models of underground cable wells play an important role in the operation and management of cities; however, the current modeling of industrial wells suffers from the problems of low modeling efficiency and incomplete 3D models. In this paper, we propose a method for modeling underground industrial wells based on the automated extraction of skeleton line and contour line features from 3D laser point cloud data. In the method, the external point cloud inside a well chamber is first separated and the skeleton points of a cable line are then extracted using the L1 median skeleton extraction algorithm with the maximum tangent sphere for the internal cable point cloud. For problems where the  $\alpha$  value in the extraction of the profile line based on the conventional alpha shape algorithm is difficult to estimate, we propose a method that combines the Delaunay triangularization and the alpha shape algorithm for extracting the profile line features of the bottom surface of the well chamber. Boundary condition checking and curvature complexity analysis are proposed to adaptively obtain the  $\alpha$  values of different shapes of industrial wells; finally, the cables and well chambers are modeled according to the acquired skeleton points and contour lines, respectively. In the experiments, the L1 median skeleton extraction algorithm is used to extract cable skeleton points for four types of cable with different levels of point cloud completeness, different levels of sparseness, different cable bending degrees, and the existence of missing point clouds, which are prominent in cable bending and turning areas. Boundary condition checking and curvature complexity analysis are carried out to calculate four typical cable wells, and the proposed  $\alpha$  value is obtained to extract the bottom surface contour line features. The height parameter of the underground cable wells is combined with the acquired contour lines to reconstruct the underground cable wells in three dimensions. The underground cable well model is highly consistent with the real object in terms of geometry and dimensions and performs well in generating details of the cables. Underground cable well modeling is crucial to improving urban infrastructure management, ensuring safety,

---

\*Corresponding author: e-mail: [201804010125@bucea.edu.cn](mailto:201804010125@bucea.edu.cn)  
<https://doi.org/10.18494/SAM5412>

optimizing maintenance, supporting emergency response, and improving decision-making efficiency, which helps achieve smart city development.

## 1. Introduction

With the acceleration of urbanization, the data quality of underground pipe networks, which are the lifeline of cities, is critical to urban function and disaster prevention.<sup>(1,2)</sup> Urban pipeline networks' deteriorating service quality necessitates the implementation of transformational strategies that will increase their operational effectiveness and quality. 3D laser scanning technology can quickly acquire 3D point clouds of underground cable tunnels, providing data support for establishing an accurate underground cable management information platform.<sup>(3,4)</sup> Efficient and accurate underground work well models can improve the visualization and efficiency of urban distribution network management and meet the needs of urban management and development. Underground cable well modeling is essential to ensuring the safety of urban infrastructure, improving cable maintenance efficiency, and optimizing urban planning and emergency response. It helps accurately locate cable routes, prevent construction damage, support asset management, and promote the development of smart cities.

The majority of domestic pipeline network information systems currently exist as an integrated secondary development system that combines large-scale, basic geographic information system software and visualization development language from both home and international sources. An underground pipeline network crisscrosses, making it impossible for two-dimensional visualization to depict the spatial relationships among pipelines. It is unnatural to have a segment of a pipeline perpendicular to the ground represented merely by a point and related notes on the plan view when certain pipes are undulating up and down. Researchers have performed the 3D model reconstruction of subterranean pipes using virtual reality and 3D visualization technologies; however, the speed of manual modeling is low and large-scale subterranean pipeline facility model development is challenging.<sup>(5)</sup> Scholars have proposed a segmented incremental extrapolation model calculation approach; nonetheless, there is a need to improve the 3D display of a limited range of exceedingly complex pipelines,<sup>(6)</sup> Scholars have designed and implemented a true 3D well room–3D data model and an automatic modeling method, but they did not include the topological relationships among pipelines and their components;<sup>(7)</sup> Scholars have used constructive solid geometry (CSG) and close-range photogrammetry to rebuild 3D pipeline models; nevertheless, reconstructing subterranean pipes is challenging and does not entail managing pipelines across a broad variety of locations. The method does not include large-scale pipeline management.<sup>(8,9)</sup> Scholars have also employed an enhanced A\* path-finding algorithm to identify optimal paths, which are then used as the skeleton of cables.<sup>(10)</sup> However, in a complex cable network, the algorithm may encounter a local optimal solution, leading to a loop, or become unable to converge to the global optimal solution. Scholars have proposed an LI-based approach that incorporates an improved adaptive k-means algorithm.<sup>(11)</sup> Clustering bootstrapping is not a viable approach to extracting the median skeleton. Similarly, while a median skeleton extraction algorithm exists, it is susceptible to forming a local skeleton closed loop when the interior of the local point cloud is missing.

Scholars have proposed a multilevel minimum bounding rectangle-based method to extract building contour lines, but this method is only suitable for extracting regular rectangular building contour lines and therefore not universally applicable.<sup>(12)</sup> Scholars have proposed a minimum spanning tree algorithm with the extended Kruskal algorithm to construct the minimum spanning graph; however, the classification of its boundary point relies on the accuracy of the boundary probability, which may be misclassified if the boundary probability is inaccurately estimated.<sup>(13)</sup> The process of deriving 3D alpha shapes from the underlying Delaunay triangulation is modified by adding additional constraints.<sup>(14)</sup> Scholars have used an improved 3D alpha shape algorithm to construct a data pyramid consisting of multiscale point layers and extracted ground points using top-down multiscale triangulated irregular network encryption.<sup>(15)</sup>

In summary, the current modeling methods have certain limitations when targeting underground industrial wells, such as manual modeling, which ensures the modeling accuracy and completeness, but it is difficult to improve the modeling speed and reduces the modeling efficiency. Existing automated extraction methods cannot cope with the extraction of complex types of contour from the point cloud of industrial wells nor ensure the completeness of the extracted contours of wells with corners, tees, crosses, and other types of well. The technical route of this article is shown in Fig. 1. To balance the requirements of modeling speed and modeling completeness, in this paper, the adopted cable and well modeling method combines automated extraction and parametric modeling and the automated extraction of the cable skeleton line, the bottom surface contour line of the well with the height parameter, and the bottom surface contour line of the chamber of the well with the standard cable radius and the skeleton line of the cable modeling. The method proposed in this paper can quickly extract the required underground pipeline information from large-scale point cloud data, which provides strong data support for urban planning, infrastructure construction, and pipeline maintenance.

## 2. Data, Materials, and Methods

The experimental data used in this paper are 3D laser underground cable well point cloud data acquired by a Faro S150 3D laser scanner. The specific scanner parameters are shown in Table 1.

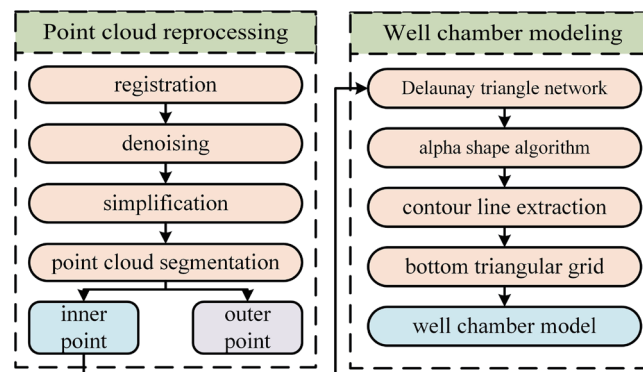


Fig. 1. (Color online) Well modeling process.

Table 1  
Scanner parameters.

Scanner parameter	Value
Scanning distance	Interior 10 m
Distance error	±2 mm
Horizontal angle	0–3600
Vertical angle	–650–900
Resolution	28.9 MPTs

Aiming at the underground cable wells with the characteristics of narrow space, low oxygen content, and complicated lines inside the wells, the advantages of using a 3D laser scanner are numerous. Firstly, the 3D laser scanner can conduct accurate measurements without directly contacting the surface of the object, which on the one hand helps protect the wells from damage, and on the other hand, ensures the safety of the operating personnel. Secondly, the 3D laser scanner can obtain 3D coordinate information quickly with high accuracy, and the minimum measurement accuracy can reach the millimeter order, which can capture the details of the object surface, measure the complex cable lines and pathways inside the cable wells, and collect the data of whole elements.

In this paper, we focus on the following four types of cable well in terms of the shape of pathways for experiments: straight-through, corner, tee-type, and four-way cable wells. The point clouds of the four types of cable well are shown in Fig. 2.

In modeling, although the geometries of the four different channel types of cable wells are different, they share some basic characteristics: the top and bottom surfaces are the same, and the sides are vertically stretched surfaces. From these common characteristics, we can obtain the contour lines of the point cloud of the bottom surface of the cable wells and the heights of the cable wells, and then construct the 3D models of the cable wells by stretching operations.

The two primary categories of noise sources for industrial wells are internal and external. The primary interior sources are as follows:<sup>(16)</sup> (1) noise points generated by internal moisture and water mist laser reflection; (2) noise points generated by laser reflection caused by internal dust particles; (3) scanner. When working, the noise points generated by jitter can be caused by humans or self-caused reasons. Radius outlier removal is carried out to filter the number of adjacent points in the point cloud space point radius range. According to the characteristics and existence form of noise points in the construction well, the radius  $R$  is set. If the set effective point does not have more than 2 adjacent points within the specified radius  $d$ , then points A and B are regarded as discrete points and will be used during denoising. The noise point form and denoising results for the work well after the elimination of the noise effect are shown in Fig. 3. The methods mainly focused on for streamlining and filtering point cloud data are the bounding box method,<sup>(17,18)</sup> geometric image streamlining method,<sup>(19,20)</sup> curvature streamlining method,<sup>(21)</sup> and normal precision streamlining method.<sup>(22,23)</sup> In this study, we use octree downsampling to divide the 3D space into eight subspaces.<sup>(24)</sup> The bounding box method removes the point cloud outside the box by constructing a bounding box. Its advantages are its simple operation and high calculation speed. Its disadvantages are that it cannot handle complex shapes and may lose important features. The geometric image simplification method simplifies points on the basis of

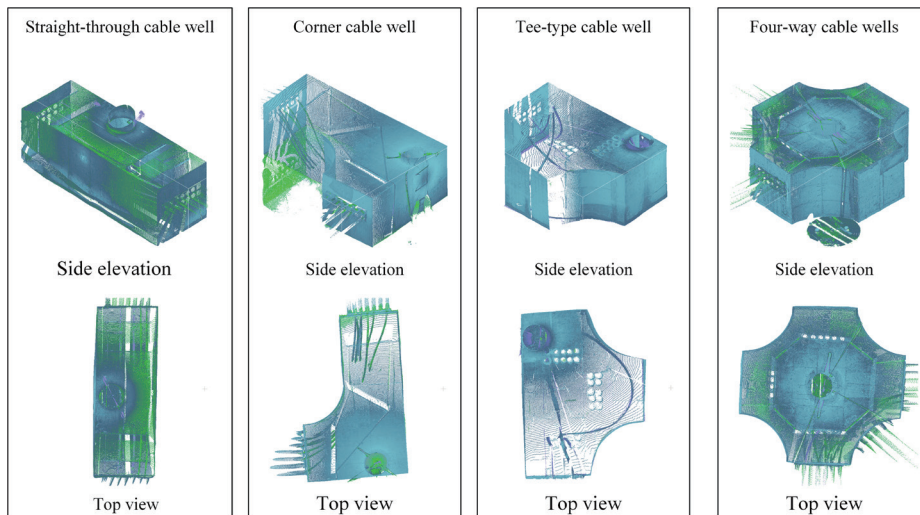


Fig. 2. (Color online) Experimental well data.

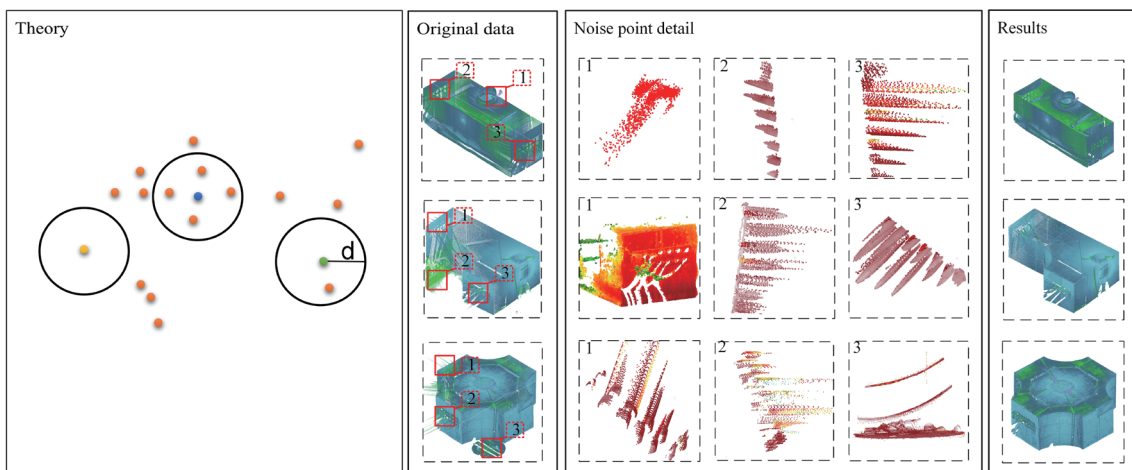


Fig. 3. (Color online) Noise point treatment for work wells.

the geometric features of the point cloud. Its advantage is that it maintains the shape well. Its disadvantages are its high calculation complexity and sensitivity to parameters. The curvature simplification method simplifies the point cloud on the basis of the local curvature of the point cloud. Its advantage is that it can retain the shape features. Its disadvantages are that it is sensitive to noise and involves a large amount of calculation. The normal accuracy simplification method simplifies the point cloud on the basis of the normal information of the point cloud. Its advantage is that it can effectively retain surface features. Its disadvantages are that the normal estimation is complex and sensitive to noise and occlusion. In point cloud downsampling, octrees can be used to quickly determine the point cloud density in each subspace and decide which points need to be retained and which points need to be deleted on the basis of the set sampling rate.

To subsequently model cables and cable wells more intuitively and easily, the processed point cloud needs to be segmented internally and externally.

Principal component analysis (PCA) transforms the data into a new coordinate system through an orthogonal transformation such that the first largest variance of any projection of the data is at the first coordinate and so on. This method is used to determine the main axis direction in point cloud data processing because it can effectively capture the main changing trends in the data. The reason for choosing PCA to determine the main axis direction of the point cloud is that it can significantly reduce the dimensionality of data while retaining the most important geometric features. PCA determines the principal axis by identifying the direction of maximum variance in the data, which makes it ideal for extracting key structural information in point cloud data. In addition, PCA has the advantages of high computational efficiency and easy implementation, making it the preferred method for point cloud feature extraction and shape analysis.

The original point cloud was processed by PCA,<sup>(25)</sup> a commonly used data degradation and feature extraction technique that identifies the main directions of change in the data and projects the data in these directions to achieve data compression and simplification.<sup>(26)</sup>

For the point cloud, suppose there are  $M$  sample points  $\{X^1, X^2, \dots, X^M\}$ . Each sample point has 3D features  $X^i = \{x_1^i, x_2^i, x_3^i\}$ , and each feature  $x_j$  has its own eigenvalue.

To eliminate the impact of translation on the data position, the data must first be centered, that is, the mean of the data is subtracted to ensure that the mean of the data is zero. The mean of the

features is  $\bar{x}_1 = \frac{1}{M} \sum_{i=1}^M x_1^i$ ;  $\bar{x}_2 = \frac{1}{M} \sum_{i=1}^M x_2^i$ ;  $\bar{x}_3 = \frac{1}{M} \sum_{i=1}^M x_3^i$ .

Then, the covariance matrix of the centered data is obtained by calculating Eq. (1). The covariance matrix is symmetric with each element representing the correlation between the corresponding dimensions. The diagonal elements are the variances in each dimension, and the off-diagonal elements represent the covariances between different dimensions.

$$C = \begin{cases} \begin{bmatrix} cov(x_1, x_1) & cov(x_1, x_2) \\ cov(x_2, x_1) & cov(x_2, x_2) \end{bmatrix} \\ cov(x_1, x_2) = \frac{\sum_{i=1}^M (x_1^i - \bar{x}_1)(x_2^i - \bar{x}_2)}{M - 1} \end{cases}, \quad (1)$$

where the relationship between the eigenvalue  $\lambda$  of the covariance matrix  $C$  and its corresponding eigenvector  $u$  is shown as:

$$Cu = \lambda u. \quad (2)$$

The PCA method determines the direction of the major axis from the direction in which the dispersion of its data is greatest, and the measure of dispersion is reflected by its sample variance  $s$ , which is obtained by calculating Eq. (3).

$$s \triangleq \frac{1}{n} \sum_{i=1}^n x_i - \bar{x}^2 \quad (3)$$

This process can determine the sample variance along the  $x$ -,  $y$ -, and  $z$ -axes to obtain the axial direction of the point cloud in the three directions.

The boundary information of each face of the model is obtained through the PCA method, the point cloud of each face is segmented, and the point cloud that does not belong to the face is eliminated by judging the normal. Taking the tee-type well as an example, Fig. 4 shows the segmentation effect of the internal and external point clouds of the tee-type well. The blue part of the point cloud is the external point cloud of the work well, and the rest of the colored part is the internal point cloud of the work well, and the colored part is divided according to the color intensity of the point cloud at the time of scanning.

### 3. Work Well Modeling Based on Automatic Extraction of Contour Features

#### 3.1 Determine the main axis direction of the point cloud

On the basis of the PCA method in Sect. 2, the point cloud of industrial wells that has been separated from the original point cloud is processed. The PCA method is conducted to obtain the boundary information of each face of the model, which is used to obtain the corresponding parameters of each face to split the point cloud of each face, and the sample variance of the point cloud along the  $x$ -,  $y$ -, and  $z$ -axes is determined to obtain the three axial directions.<sup>(27,28)</sup> The results of the PCA screening of the main axis direction are shown in Fig. 5.

On the basis of the PCA-determined principal axis direction, a random sampling consistency algorithm was used to fit the planar model on the basis of the characteristics of the cable well point cloud,<sup>(29)</sup> and outlier points were removed by iteration, thus separating the bottom surface

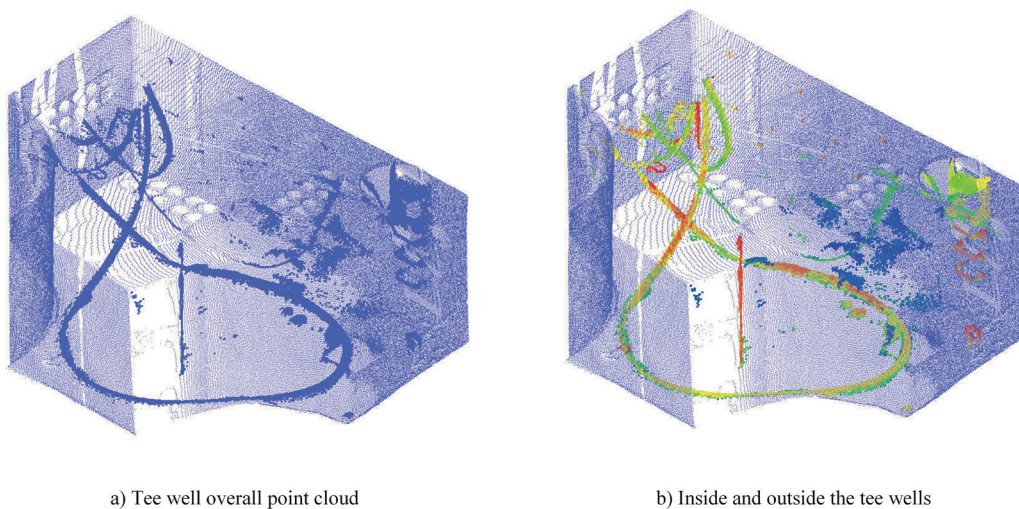


Fig. 4. (Color online) Segmentation of internal and external point clouds of tee shafts.

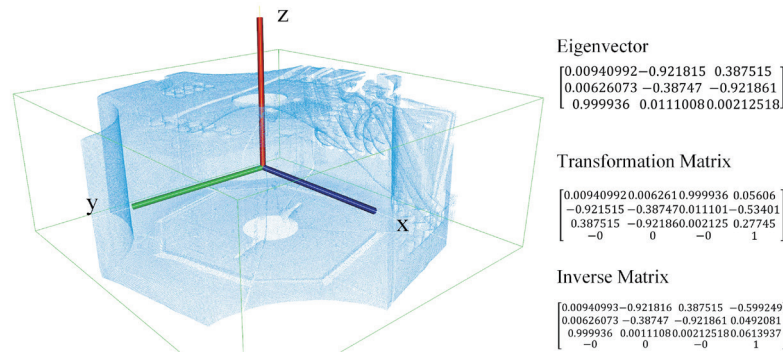


Fig. 5. (Color online) PCA filter spindle direction.

and non-bottom surface points in the point cloud. The planar fit was optimized by centering the point cloud coordinates. Since the separated point cloud may have missing cases, fitting through the plane was conducted according to the fitting parameters in the overall point cloud to extract a certain distance threshold from the plane of the point cloud, and the threshold for a number of iterations of processing was gradually reduced to obtain the final point cloud data of each surface without missing cases. The steps are as follows:

- (1) Calculate the normal vector: search for the proximity of individual points in the point cloud, fit it and the neighboring points into a surface, and find the eigenvector corresponding to the smallest eigenvalue of the point in the surface according to the result of PCA in the previous step, and this eigenvector is the normal vector of the fitted surface.
- (2) Perform iterative model estimation using a random sampling consistency algorithm to estimate the data model parameters from the point cloud.
- (3) Points identified as bottom surfaces are extracted and re-stored.

The effect of segmenting the individual surfaces of the well chamber is shown in Fig. 6.

### 3.2 Work well contour line extraction

When dealing with the contour lines of the projected surface of an industrial well, straight-through wells are usually presented as regular straight-line geometries; however, corner, tee-type, and four-way wells contain curved parts, which makes it difficult to accurately reflect the real geometrical characteristics of the wells with the traditional feature point extraction and fitting methods. In this paper, the alpha shape algorithm combined with the Delaunay triangular mesh is used to extract the contour lines of the bottom surface of the well. Owing to the effect of the point cloud of the wellhead and small components inside the bottom surface of the industrial well, it is necessary to first establish a Delaunay triangular mesh for the point cloud and then start to judge from the outer boundary of the triangular mesh.<sup>(30)</sup>

The basic idea of the alpha shape algorithm is to roll a circle of radius alpha around a given set of discrete points,  $S$ . As shown in Fig. 7, when radius is taken appropriately, this circle does not roll into the interior of  $S$ . The points intersecting the circle are the edge contour points of  $S$ , and the traces of its rolling are the contour lines of  $S$ .<sup>(31)</sup>



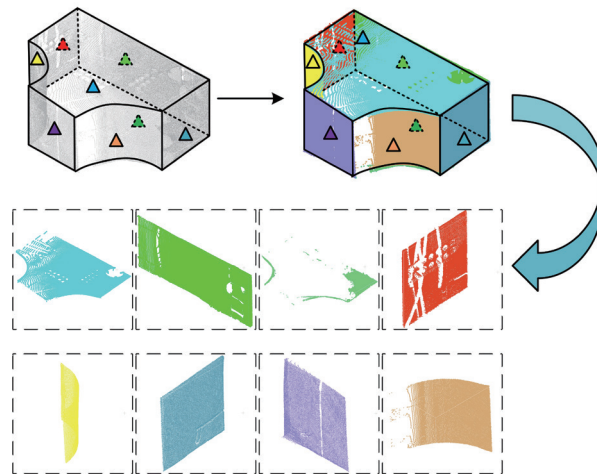


Fig. 6. (Color online) Plane segmentation results for work well point cloud.

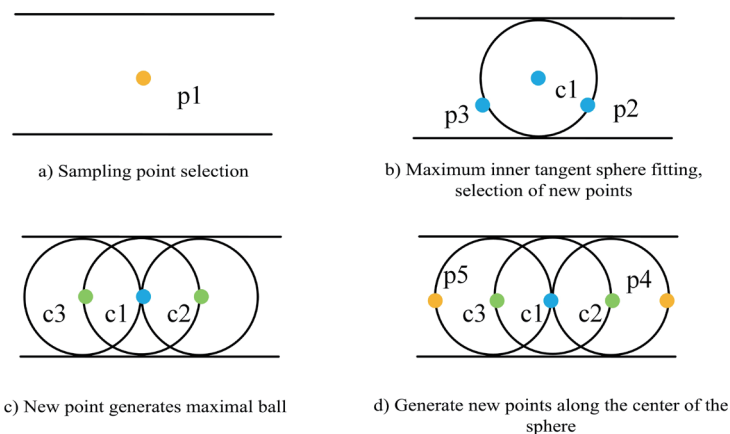


Fig. 7. (Color online) Alpha shape algorithm with maximum inscribed sphere.

Take any two points  $p_1$  and  $p_2$  within the point set  $S$ , set a discriminant radius  $\alpha$ , and draw a circle with the radius  $\alpha$  along the outer boundary of the triangular mesh. If there is no other data point inside any circle, points  $p_1$  and  $p_2$  are considered the contour points, and the center of the circle over the two points can be obtained as  $p_3$ , and the formula for  $p_3$  is shown in Eqs. 8 and 9. The alpha shape algorithm overcomes the disadvantage of the effect of the shape of the boundary points of the point cloud and can extract the boundary points quickly and accurately. When the distance between two edges is within a certain threshold, and the angle between them is within a certain range, it can be considered that they belong to a straight line.

$$\begin{cases} x_3 = x_1 + \frac{1}{2}(x_2 - x_1) + H(y_2 - y_1) \\ y_3 = y_1 + \frac{1}{2}(y_2 - y_1) + H(x_2 - x_1) \end{cases} \quad (8)$$

Among them,

$$H = \sqrt{\frac{\alpha^2}{S^2 p_1 p_2} - \frac{1}{4}}, S^2 p_1 p_2 = (x_1 - x_2)^2 + (y_1 - y_2)^2. \quad (9)$$

The contour lines of the work wells obtained by combining the Delaunay triangular mesh and the alpha shape algorithm are shown in Fig. 8, with details of the Delaunay triangular mesh illustrated in Figs. 1 and 2.

The alpha shape algorithm involves the determination of the  $\alpha$  value, but the choice of the  $\alpha$  value is difficult to estimate in practice. To reduce the inaccuracy of the contour line extraction results due to human error, this paper employs boundary condition checking and curvature complexity analysis to compute a proposed  $\alpha$  value adaptively. Boundary condition checking finds a minimum  $\alpha$  among a series of  $\alpha$  values so that the generated contour lines have specific properties: (1) contain a specified number of connected components and (2) all data points are at the boundary or inside the shape.

The steps to obtain the adaptive  $\alpha$  value by applying boundary condition checking and curvature complexity analysis calculations are as follows.

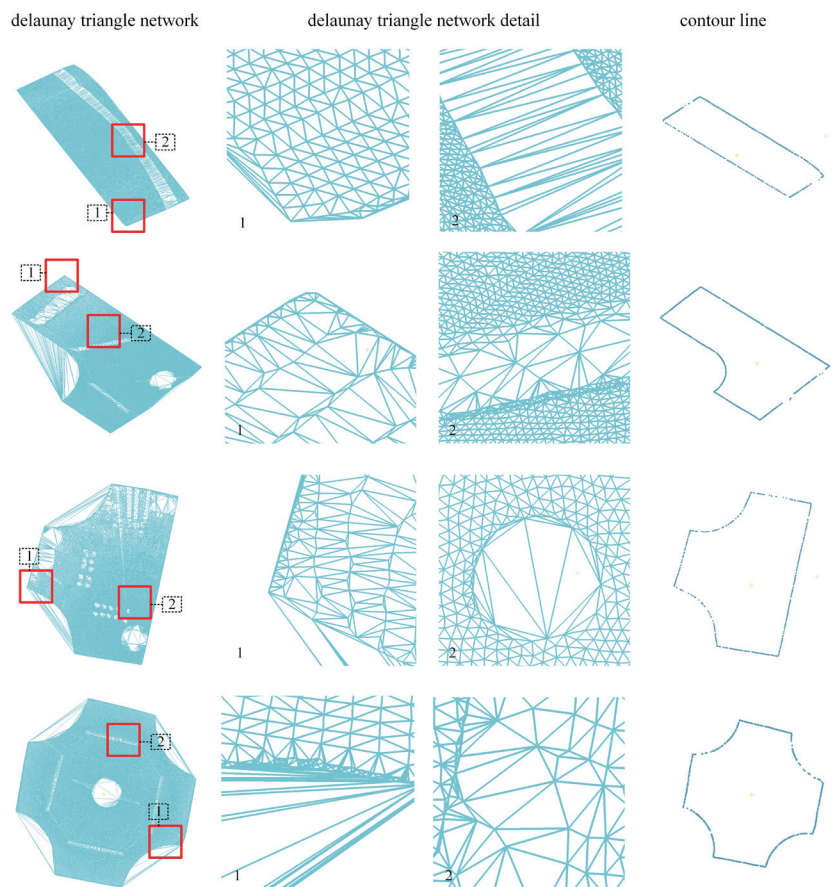


Fig. 8. (Color online) Contour point cloud extraction results.

- (1) Determine the upper limit  $\alpha_{max}$  and lower limit  $\alpha_{min}$ . Since the experimental datasets in this paper are all well-structured physical point cloud models, and considering the constraints of the skeleton extraction on the number of regions, here we set  $\alpha_{min} = 0.001$  and  $\alpha_{max} = 1.0$ .
- (2) For each point, the bisection finding method is used to check whether it can be connected to other points through the triangles that satisfy the  $\alpha$ -value condition to determine the connectivity component of the point cloud and to ensure that all the data points are at the boundary or inside of the shape. In this paper, we extracted the external contour line of the point cloud of the industrial wells; therefore, we set the connectivity component to 1 and obtained  $\alpha_1$  between the upper limit of  $\alpha_{max}$  and the lower limit of  $\alpha_{min}$ .
- (3) In increments from  $\alpha_1$  to  $\alpha_{max}$ , calculate the curvature complexity under different values of  $\alpha$  and plot the curve graph.
- (4) The curvature value corresponding to the inflection point on the way down the curve graph can indicate the current contour line curvature at the optimal curvature, whereas the value larger than this curvature corresponds to the contour line corner points and the wrongly extracted interior points.
- (5) According to the number of corner points and the degree of pathway curvature of the contour lines at the bottom of different workings, their corresponding curvature that should have the complexity of the  $\alpha$  value is evaluated to get the adaptive optimal  $\alpha$  value.

As shown in Fig. 9, the curvature at the inflection point of the contour line point cloud with different values of  $\alpha$  is 0.1, and it is proved by experiments that it is more appropriate to take 0.1 as the threshold value for the curvature complexity calculation. Figure 10 shows the curvature comparison of different positions of the contour line point cloud. It can be seen that the curvature at the corners of the contour line is larger, and the curvatures of the straight and curved parts of

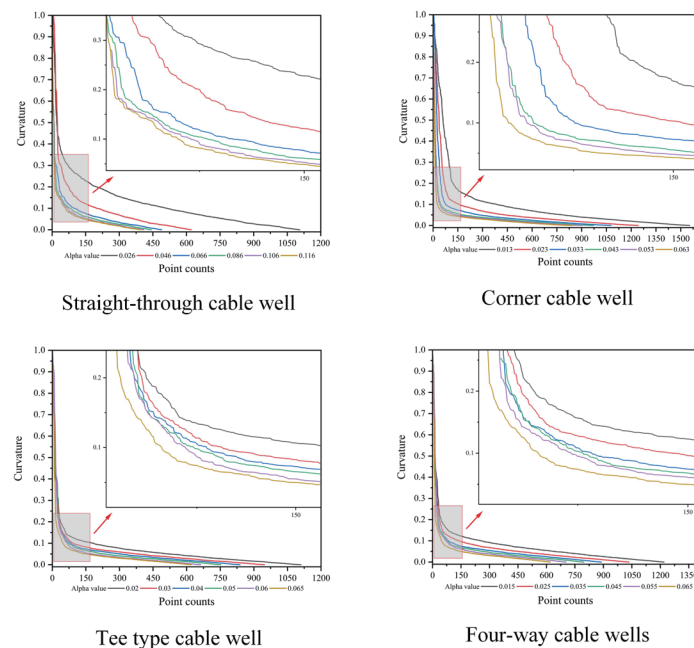


Fig. 9. (Color online) Curvature of contour point cloud under different  $\alpha$  values.

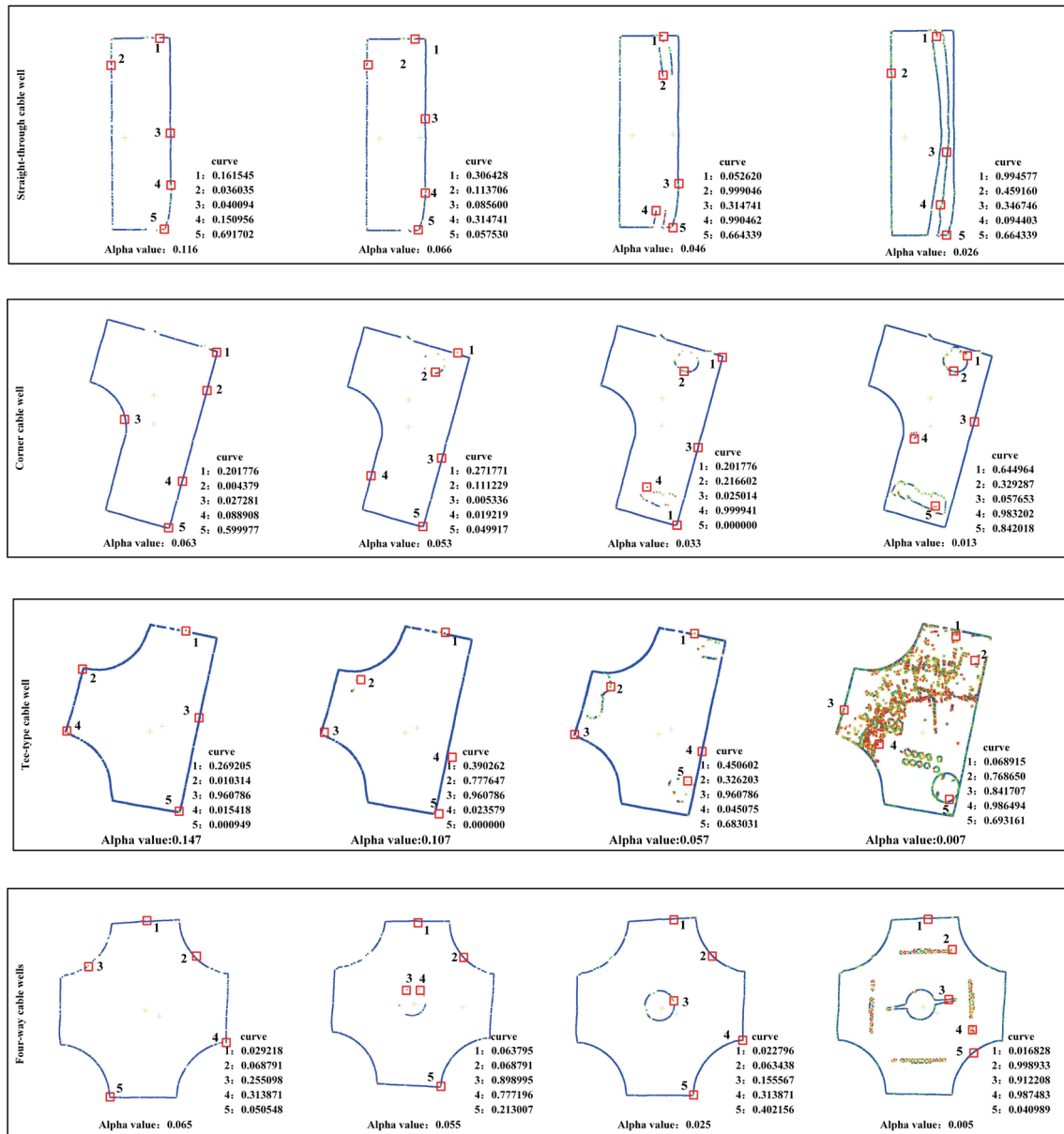


Fig. 10. (Color online) Comparison of curvatures at different positions of contour point cloud.

the contour line are basically consistent, but the curvature distribution of the internal points is messy owing to the improperly selected  $\alpha$  value. Therefore, the adaptive optimal  $\alpha$  value can be obtained by limiting the complexity of the curvature.

#### 4. Results

Figure 11 shows the results of underground well chamber modeling. The contour extraction of each well chamber is highly consistent with the actual point cloud data, and the peripheral model of the well chamber also shows good modeling effect, which means that the model can

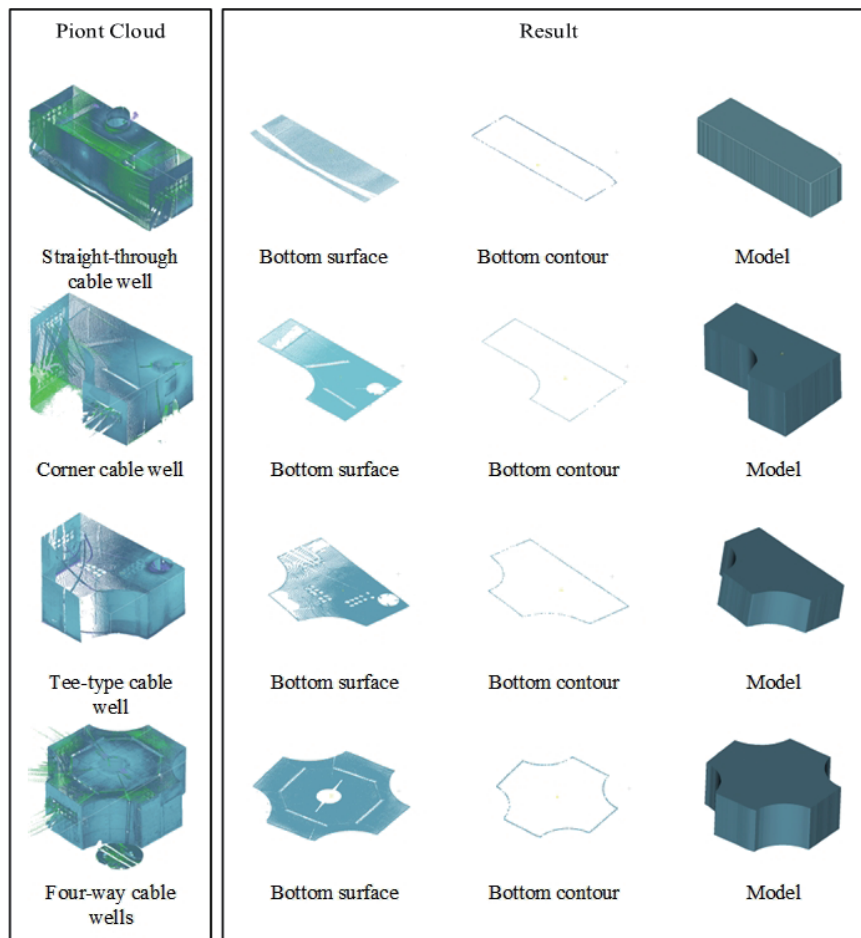


Fig. 11. (Color online) Well modeling results.

accurately reflect the actual situation of the underground well chamber in terms of not only the geometric shape but also the spatial position.

The four types of work well data used in underground work well chambers have their own characteristics, so different alpha values need to be set for different work wells. Taking the three-way well as an example, as shown in Table 2, when the alpha value is 10, the contour line of the bottom point cloud will be incompletely extracted and the point cloud features cannot be displayed. When the alpha value is set to 0.01 and 0.001, the contour of the internal components such as the wellhead will be extracted. Therefore, when extracting the contour line of the work well, it is necessary to select a suitable alpha value to extract the appropriate contour line.

The alpha value controls the geometric features of the generated shape and indicates the thickness of the generated shape. The larger the alpha value, the simpler the generated shape and the fewer the geometric features, whereas the smaller the alpha value, the more complex the generated shape and the more details can be captured. This paper uses different alpha values for different well data according to the density and distribution of point cloud data. The specific settings are shown in Table 3.

Table 2  
(Color online) Contour results extracted with different alpha values.

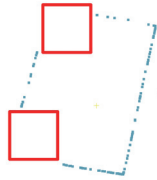



Alpha value	10	0.1	0.01	0.001
Bottom contour				

Table 3  
Work well contour extraction alpha value setting.

Type	Straight-through cable well	Corner cable well	Tee-type cable well	Four-way cable wells
Original data count	39736	53932	37945	75032
Contour count	395	844	612	620
Adaptive alpha value	0.116	0.063	0.147	0.065
Contour extraction time	0.326499	0.46657	0.298375	0.663932

Table 4  
(Color online) Comparison of contour extraction methods.





















	Original data	Mesh generation	Normal estimation	Alpha shape	Methods
Straight-through cable well					
Time (s)	-	0.160583	28.161530	2.687087	0.326499
Point count	39736	10418	2078	804	395
Tee-type cable well					
Time (s)	-	0.136134	25.161718	2.384653	0.298375
Point count	37945	6312	2688	767	612
Four-way cable wells					
Time (s)	-	0.150922	61.322852	4.871719	0.663932
Point count	75029	2059	3998	804	620
Tee-type cable well					
Time (s)	-	0.150684	43.367463	3.344963	0.46657
Point count	53932	4539	4330	654	844

Table 5

Comparison of the satisfactory rates of different methods of contour line extraction in four-way wells.

Method	Manual Point selection	Mesh generation	Normal estimation	Alpha shape	Methods
Point count	1179	2059	3998	804	620
Qualified points		15	728	491	459
Satisfactory rate		0.728509%	18.209105%	61.069652%	74.032258%

The alpha shape algorithm combined with the Delaunay triangulation adopted in this paper is more suitable for the contour line features of the well chamber with interlaced straight lines and curves. Compared with other algorithms, it has a better contour line extraction effect, and the specific comparison is shown in Table 4. It can be seen that the contour line extracted by the mesh division method contains a large number of internal points, and the normal estimation method cannot distinguish between the internal boundary and the external contour line, and neither can be used as the contour line basis for well chamber modeling. The method proposed in this paper can extract contour line point clouds with complete shapes and no interference from small component contours, which is better than the extraction time of the traditional alpha shape algorithm method in terms of time.

To verify the superiority of the method proposed in this paper over other methods, taking the four-way well point cloud as an example, 1179 bottom contour points were selected manually. Contour points were obtained by the proposed algorithm of the grid division method and the normal estimation method and the alpha shape algorithm method. If the selected contour points were within the manually selected points, then they were recorded as qualified points, and the satisfactory rates of the different methods were obtained and are shown in Table 5. Combined with the contour point extraction times of different methods in Table 4, it can be proved that the method proposed in this paper is superior to the other methods in terms of speed and quality.

## 5. Conclusion

To overcome the inapplicability of existing skeleton line extraction methods to model industrial well cables and the inefficiency of manual industrial well modeling, in this study, we developed an automated underground pipeline modeling method, which is based on 3D laser point cloud data, and effectively improved the modeling efficiency and accuracy of industrial well cables. In this method, the internal and external point clouds of the industrial wells are first separated, and the point cloud data are then processed using principal component analysis and combined with the Delaunay triangulation and alpha shape algorithms to extract the contour lines of the work wells. The following results were from experimental tests:

- (1) For four types of typical cable well in the construction well chamber, in this paper, we used boundary condition checking and curvature complexity analysis to compute the proposed alpha value adaptively. Compared with the traditional alpha shape algorithm method, which requires changing the alpha value one by one to adapt to different data characteristics, the method proposed in this paper can automatically change the alpha value to calculate the contour lines and the curvature of the contour lines until the curvature meets the curvature

characteristics of the contour lines of the different data, which enables the quick and accurate determination of a complete point cloud of the contour lines that retains the characteristics of the well chambers.

- (2) However, the proposed algorithm also has some limitations, especially when dealing with the mutual occlusion of cable point clouds and the modeling of small components in well chambers. How to effectively separate the adherent cable point clouds and accurately extract the features of small components are difficult problems that need to be tackled in the subsequent research.

### Acknowledgments

This research was funded by the National Natural Science Foundation of China (42171416).

### References

- 1 Z. Xie, F. Jiang, J. Xu, Z. Zhai, J. He, D. Zheng, J. Lian, Z. Hou, L. Zhao, Y. Wang and Y. Feng: Sustainability **15** (2023) 10067. <https://doi.org/10.3390/su151310067>
- 2 Q. Li, Y. Yang, B. Yu, and X. Hu: Adv. Build. Technol. **II** (2002) 1629. <https://doi.org/10.1016/b978-008044100-9/50201-1>.
- 3 Z. Gao, F. Li, Y. Liu, Y. Su, Z. Fang, M. Yang, Y. Li, J. Yu and Q. Zhang: Opt. Lasers Eng. **126** (2020) 105879. <https://doi.org/10.1016/j.optlaseng.2019.105879>.
- 4 C. Wu, Y. Zhou, X. Jiang, Y. Xu, X. Wang and H. He: 2018 Third Int. Conf. Security of Smart Cities, Industrial Control System and Communications (SSIC)(IEEE, 2018) 8556679.
- 5 Z. He and Z. Ma: Proc. 2009 First Int. Conf. Information Science and Engineering (2009) 2161.
- 6 Q. Li, Y. Yan, B. Yang and X. Hua: Int. J. Sustainable Build. Technol. Urban Dev. **2** (2002) 1629. <https://doi.org/10.1016/b978-008044100-9/50201-1>.
- 7 W. Si, Y. Yang, M. Wang, and Y. Chen: J. Surv. Mapp. Sci. Technol. **33** (2016) 400.
- 8 T. Burger and W. Busch: Int. Arch. Photogramm. Remote Sens. **33** (2000) 107.
- 9 E. Pernkopf: Int. Arch. Photogramm. Remote Sens. **33** (2000) 215.
- 10 Z. Feng: Master's Thesis, Tianjin University of Technology (2023). <https://doi.org/10.27360/d.cnki.gtjgy.2023.000209>.
- 11 B. Lu and X. Fang: Acta Autom. Sin. **48** (2022) 1994. <https://doi.org/10.16383/j.aas.c200284>.
- 12 G. Liu, K. Liu, H. Ma, L. Zhang, and J. Yuan: Laser Optoelectron. Prog. **61** (2024) 456.
- 13 G. Bendels, R. Schnabel, and R. Klein: Journal of WSCG (2006).
- 14 W. Zhou and H. Yan: Briefings Bioinf. **15** (2014) 54. <https://doi.org/10.1093/bib/bbs077>.
- 15 D. Cao, C. Wang, M. Du, and X. Xi: Remote Sens. **16** (2024) 1443. <https://doi.org/10.3390/rs16081443>.
- 16 Z. Ren, R. Yuan, L. Wang, H. Deng, W. Wang, J. Zhang: Coal Sci. Technol. 1-15 (2024-08-07). <http://kns.cnki.net/kcms/detail/11.2402.TD.20240323.1416.002.html>.
- 17 F. Liu, Y. Ren, C. Liu, and F. Jin: J. Syst. Simul. **24** (2012) 1980.
- 18 M. Zhang, Z. Feng, J. Guo, and L. Ji: J. Shanghai University (Nat. Sci. Ed.) **11** (2005) 242.
- 19 B. Sun, J. Liu, X. Zhang, and W. Sun: J. Xi'an Jiaotong University **44** (2010) 38.
- 20 B. Zhou, Y. Cheng, and Z. Gu: Mod. Manuf. Eng. **67** (2008) 64.
- 21 D. Liu, J. Chen, J. Guo, L. Ju: Shanghai University (Nat. Sci. Ed.) **35** (2008) 334.
- 22 Z. Chen and F. Deng: Acta Opt. Sin. **33** (2013) 0815001. <https://doi.org/10.3788/aos201333.0815001>.
- 23 D. Shen, C. Zhang, Z. Fan, and Y. Liu: China Mech. Eng. **20** (2009) 2840. <https://doi.org/10.3901/jme.2019.19.146>.
- 24 C. Sun, H. Yuan, X. Mao, X. Lu and R. Hamzaoui : IEEE Signal Process. Lett. (2024). <https://doi.org/10.1109/lsp.2024.3426918>.
- 25 Y. Zhang, W. Lin, and X. Han: Comput. Mod. **9** (2023) 59.
- 26 D. Cheng, D. Zhao, J. Zhang, C. Wei and D. Tian: Sensors **21** (2021) 3703. <https://doi.org/10.3390/s21113703>.
- 27 B. Fan, J. Yao, and Z. Lin: Surv. Mapp. Sci. **11** (2021) 3703.
- 28 H. Liu, S. Wang and D. Zhao: Optik **243** (2021) 166856. <https://doi.org/10.1016/j.jjleo.2021.166856>.
- 29 B. Zhao, J. Yuan and D. Wang: J. Comput. Appl. **31** (2011) 1053. <https://doi.org/10.3724/sp.j.1087.2011.01053>.
- 30 X. Lai: Remote Sens. **14** (2019) 1636. <https://doi.org/10.3390/rs11141636>.
- 31 H. Edelsbrunner and E.P. Mücke: ACM Trans. Graph. **13** (1994) 43. <https://doi.org/10.1145/174462.156635>.



## About the Authors



**Ming Huang** is a professor and Ph.D. supervisor at Beijing University of Civil Engineering and Architecture. His research interests are in point cloud and image hyperfine 3D modeling and visualization, and mobile vehicle laser point cloud ground feature intelligent recognition.

([huangming@bucea.edu.cn](mailto:huangming@bucea.edu.cn))



**Mingyue Kuang** is a graduate student at the School of Geomatics and Urban Spatial Informatics, Beijing University of Civil Engineering and Architecture. Her research involves point cloud processing and 3D modeling.

([201804010125@bucea.edu.cn](mailto:201804010125@bucea.edu.cn))



**Rui Wu** received his master's degree from Hefei University of Technology, P.R. China. Now, he works at the School of Architecture and Civil Engineering, Huangshan University, and he studies at the School of Geomatics and Urban Spatial Informatics, Beijing University of Civil Engineering and Architecture. His research interests include architectural design and its theory, historical building and protection, green building, and city planning.

([1108130122005@stu.bucea.edu.cn](mailto:1108130122005@stu.bucea.edu.cn))